Please cite this paper as: T. Wang, D. Zheng, K. Vegso, G. Baillard, P. Nadazdy, N. Mrkyvkova, P. Siffalovic, Y. Chen, L. Coolen, Th. Pauporte, F. Feng, A Dual Strategy to Enhance the Photoelectric Performance of Perovskite-Based Photodetectors for Application in Optical Communications. Chem. Eng. J. 488 (2024) 151068. https://doi.org/10.1016/j.cej.2024.151068.

A Dual Strategy to Enhance the Photoelectric Performance of Perovskite-Based Photodetectors for Potential Applications in Optical Communications

Tao Wang[1,2], Daming Zheng[2,3,4], Karol Vegso[5,6], Guillaume Baillard,[4] Peter Nadazdy,[5,6] Nada Mrkyvkova[5,6], Peter Siffalovic[5,6], Yimu Chen[1]*, Laurent Coolen[4]*, Thierry Pauporte[3]*, Fu Feng[1,2,7]*

1. Ministry of Industry and Information Technology Key Lab of Micro-Nano Optoelectronic Information System, Guangdong Provincial Key Laboratory of Semiconductor Optoelectronic Materials and Intelligent Photonic Systems, Harbin Institute of Technology (Shenzhen), Shenzhen, Guangdong 518055, China.
2. Nanophotonics Research Center, Shenzhen Key Laboratory of Micro-Scale Optical Information Technology and Institute of Microscale Optoelectronics, Shenzhen University Shenzhen 518060, P. R. China.
3. Chimie ParisTech, PSL Research University, CNRS, Institut de Recherche de Chimie Paris (IRCP), UMR8247, 11 rue P. et M. Curie, F-75005 Paris, France.
4. Sorbonne Université, CNRS, Institut de NanoSciences de Paris, INSP, F-75005 Paris, France.
5. Institute of Physics, Slovak Academy of Sciences, Dubravska cesta 9, 84511 Bratislava, Slovakia.
6. Center for Advanced Materials and Applications (CEMEA), Slovak Academy of Sciences, Dubravska cesta 5807/9, 84511 Bratislava, Slovakia.
7. Research Center for Humanoid Sensing, Zhejiang Lab, Hangzhou 311100, China.

*Correspondence: chenyimu@hit.edu.cn; laurent.coolen@insp.jussieu.fr; thierry.pauporte@chimieparistech.psl.eu; fufeng@szu.edu.cn.

Abstract: The emerging metal halide perovskite photodetectors (PDs) attract extensive attention for optical communications due to their excellent photoelectric properties and are considered promising alternatives for the next generation of PDs. Here, we demonstrate high-performance $MAPbI_3$ PDs based on the p-i-n structure for optical communications. A twofold approach is implemented to enhance the photoelectric performance and stability of the device. First, we introduce Au nanoparticles to reduce grain boundaries and defects, and increase the crystallinity of perovskite. Second, we use n-propylammonium iodide as an efficient recrystallization agent to decrease

Please cite this paper as: T. Wang, D. Zheng, K. Vegso, G. Baillard, P. Nadazdy, N. Mrkyvkova, P. Siffalovic, Y. Chen, L. Coolen, Th. Pauporte, F. Feng, A Dual Strategy to Enhance the Photoelectric Performance of Perovskite-Based Photodetectors for Application in Optical Communications. Chem. Eng. J. 488 (2024) 151068. https://doi.org/10.1016/j.cej.2024.151068.

interface recombination and create a capping layer of a quasi-2D $(PA)_2PbI_4$ perovskite coating. This barrier layer also protects the underlying 3D perovskite film from degradation. The prepared PDs exhibit a high responsivity of 0.4 A W^{-1}, a response time of 7.58 μs, and an on/off current ratio of 2.0×10^5. In addition, the modified PDs present outstanding long-term environmental stability (>100 days) without encapsulation under ambient conditions. Finally, the PDs are successfully integrated into a visible light communication system to transmit ASCII-encoded information as an optical signal receiver. The results open up the possibility of developing high-speed and stable metal halide perovskite PDs that have potential for applications in optical communications.

Keywords : Halide perovskite; Gold nanoparticles; n-propylammonium iodide; photodetector; optical communication; high bit rate

Introduction

Photodetectors (PDs) are optoelectronic devices capable of converting light into electronic signals. They are key components for optical interconnection systems, including optical communications, image sensing, digital display, and environmental monitoring[1-5]. For visible light communications (VLCs), PDs are required to exhibit high responsivity, fast photoelectric response, and high stability.[6-8] With the rapid development of intelligent technology infusion, VLCs have received widespread attention for their attractive characteristics of fast data transmission speed and high bandwidth. However, conventional PDs for VLCs still have many shortcomings such as limited bandwidth, low absorption coefficient, lack of on-chip integration and complex manufacturing [2, 9]. Furthermore, commercial PDs rely on high-quality active semiconductor layers, requiring precise control of material growth, high-temperature integration techniques, and high manufacturing costs[10-13]. In order to exploit the next generation of optoelectronic devices, there is an urgent need to find cost-effective and energy self-sufficient PDs to replace conventional inorganic semiconductor-based PDs.

In recent years, solution-processable metal halide perovskites have become one of the most promising candidate materials for optoelectronic devices in the semiconductor family due to a long charge carriers diffusion length, large adsorption coefficient, low density of trap states, tunable band gap and low/mild-temperature material processability[14-15]. Halide perovskites have acquired great success in the field of PDs, and have given rise to extensive researches in the field of photodetection[16-18]. They also became important materials for optical imaging and optical communications[19-21]. However, emerging lead halide perovskite optoelectronic devices still face significant challenges due to their instability to moisture, heat, and ultraviolet irradiation. Therefore, to date, there are few reports on PDs-based perovskite that simultaneously possess high responsivity, fast response, and sufficient stability, and these are critical parameters for PD applications in optical communication systems. According to

previous reports, the optoelectronic performance of PDs, especially their response speed, is closely related to the structure of PDs and the material properties of the optical absorption layer[22-24]. A number of emerging high-speed perovskite heterojunction p-i-n devices such as PEDOT:PSS/$MAPbI_3$/PCBM/C_{60} heterojunction[25], MoS_2/$(PEA)_2SnI_4$ heterojunction[26], and $(PEA)_2(MA)_2Pb_3I_{10}$/AuAgNPrisma@SiO_2[27] PDs have shown great development potential in optical communication. The structure of perovskite PDs are generally divided into two types: p-i-n diode and metal-semiconductor-metal (MSM) planar structure. Due to the use of an efficient charge barrier layer, PDs based on the p-i-n diode structure exhibit significantly reduced dark current; hence, their sensitivity and response speed are greatly improved compared to MSM counterparts. For example, Cen *et al.* reported PDs based on polycrystalline perovskite film with p-i-n structure exhibiting an ultralow dark current of 10 pA and response speed as fast as 28 μs[2]. Finally, the PDs were successfully integrated into the visible light communication system as an optical receiver for transmitting text, displaying bitrates of up to 100 kbps. In addition, for p-i-n type perovskite PDs, the charge selective layer can effectively passivate of defects, and the response time of the device can be improved down to the nanosecond level due to the internal electric field, showing enormous potential in the field of optical communication applications. Moreover, to better improve the responsivity and stability of perovskite device, the use of metal ions and Au nanoparticles as additives or passivators has been successfully demonstrated [28-30]. It led to a positive effect on the grain size, crystal morphology, crystallinity, and recrystallization of perovskite, which can reduce the surface defect density of crystal formation and improve its photoelectric performance[31-32]. For example, Liu *et al.* introduced Cu^+ into the perovskite film to improve the responsivity and photoresponse rate[33]. The optimal perovskite PDs were successfully integrated into a home-made VLC system as a light signal receiver for transmitting text and audio signals, exhibiting a promising application prospect. Although the photoelectric performance of the device can be optimized in different ways, simultaneously developing perovskite PDs that exhibit excellent photoelectric detection, fast response time and environmental stability remains a challenge in the field of optical communication.

Here we present high-performance PDs processed from $MAPbI_3$ perovskite film with a p-i-n structure. To boost the photoelectric properties and stability of the device, we propose a binary strategy that significantly improves the crystallization quality of perovskite films: (i) introducing Au nanoparticles (Au_NPs) to decrease grain boundaries and defects states density, and increase crystallinity of films, (ii) using n-propylamine hydroiodide (PAI) as a post-treatment compound to reduce interface recombination, and form a quasi-2D $(PA)_2PbI_4$ perovskite capping layer on the surface of the film notably to improve stability. The PDs have outstanding optoelectronic performance such as high responsivity and specific detectivity, fast response speed, and a wide range of spectral response. The photoelectric properties measured in this study are also the best reported among similar $MAPbI_3$ perovskite structure PDs. Moreover,

Please cite this paper as: T. Wang, D. Zheng, K. Vegso, G. Baillard, P. Nadazdy, N. Mrkyvkova, P. Siffalovic, Y. Chen, L. Coolen, Th. Pauporte, F. Feng, A Dual Strategy to Enhance the Photoelectric Performance of Perovskite-Based Photodetectors for Application in Optical Communications. Chem. Eng. J. 488 (2024) 151068. https://doi.org/10.1016/j.cej.2024.151068.

the device demonstrated excellent ambient stability, with only a slight reduction of the photoresponsivity after 100 days of storage under ambient conditions. Finally, we integrated the optimized device as an optical signal receiver into an optical communication system, for effective text transmission and demonstrating a promising application prospect.

Results and discussion

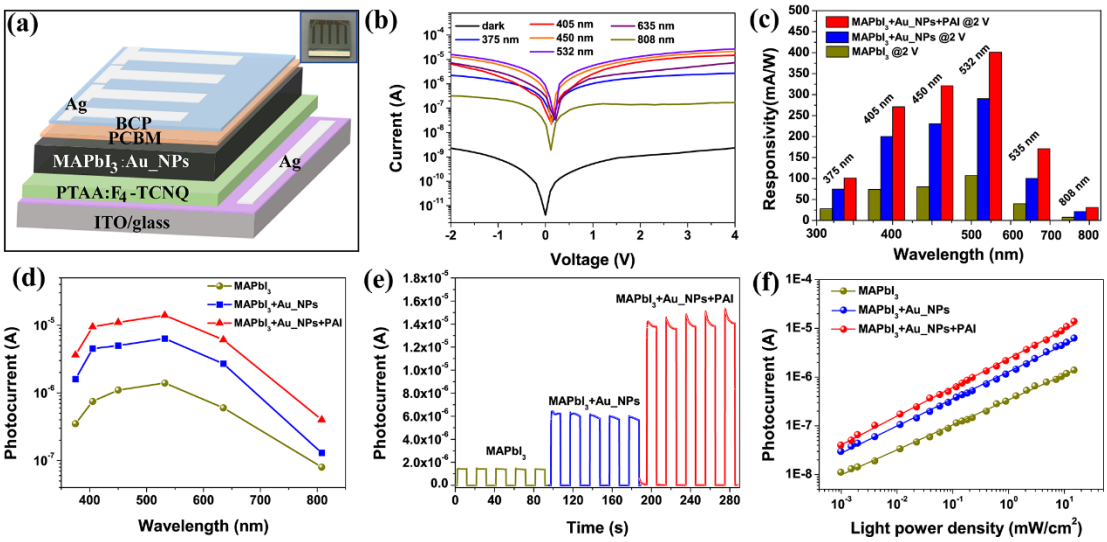

Figure 1. (a) PDs structure diagram based on $MAPbI_3$ perovskite. The inset shows the optical images of the device **(b)** The logarithmic current-voltage curves of the PVK-Au_NPs-PAI-PDs under dark and various light wavelengths (14.77 mW cm^{-2}). **(c)** The responsivity of three different device structures under different light wavelengths irradiation with a light intensity of 0.98 μW cm^{-2}. **(d)** The function of device-related photocurrent and light wavelength at 2 V bias. **(e)** Photocurrent versus time curves of all devices at 2 V bias and light intensity of 14.77 mW cm^{-2} at 532 nm. **(f)** Graph of the change of photocurrent with the light power density of all devices at a 2 V bias.

The schematic structure of the PDs is shown in **Figure 1a**. The p-type polymer poly (bis (4-phenyl)(2,4, 6-trimethylphenyl) amine) (PTAA) was used as the hole transport layer. The $MAPbI_3$ perovskite was prepared from a precursor solution. The molecules[6,6]-phenyl-C61-butyric acid methyl ester (PCBM) and bathocuproine (BCP) acted as the electron transport layer and hole-blocking layer, respectively. The detailed preparation process of perovskite PDs is shown in **Figure S1**. To satisfy PD requirements for photoelectric applications, we implemented a twofold approach that significantly enhanced the crystalline quality of the perovskite films: (i) we embedded Au_NPs into the film to reduce grain boundaries and defects and increase (re)crystallization, and (ii) we applied the PAI in isopropyl alcohol (IPA) solution for surface treatment of the perovskite layer to recrystallize the grain boundaries and inhibit

defects to reduce recombination. The PDs of $MAPbI_3$ perovskite treated with Au_NPs and PAI are denoted as PVK-Au_NPs-PAI-PDs. To optimize the device performance, we regulated the sputtering time of Au_NPs and the concentration of PAI. The results show that the device performance reached its optimal level when the sputtering time of Au_NPs was 15 s, and the PAI concentration was 4 mg mL^{-1}. The details of PD manufacturing process optimization can be found in the supporting information (**Note 1**, **Figures S2**, **S3 and S4**). The thickness of the optimized perovskite film was measured at approximately 270 nm on the scanning electron microscopy (SEM) cross-sectional views (see **Figure S4,** Supporting Information).

The photo-response of the device was studied to evaluate its optoelectronic performance. The logarithmic current-voltage curves of the PDs at different incident wavelengths in **Figure 1b** demonstrate a wide spectral response range. The maximum photocurrent was found at a wavelength of 532 nm. Next, we further investigated the photoelectric performance to evaluate the detectability of the modified device. Under illumination, the built-in electric field can extract the photogenerated electron-hole pairs, resulting in significantly improved conductance. **Figure 1b** shows the logarithmic I-V curves of the PDs obtained in the dark and under light illumination at various wavelengths. It should be noted that although the p-i-n photodiode structure is adopted, rectifier characteristics of the device are not obvious, which can be attributed to the addition of gold particles that increases the conductivity of the perovskite and weakens the rectification phenomenon.[28, 31]. The dark current value of the PDs was 1.0 × 10^{-9} A at a 2 V bias voltage, while, at the light intensity of 14.77 mW cm^{-2}, the photocurrent increased up to 1.4 × 10^{-5} A at 532 nm. **Figure 1c** shows the photoresponsivity (*R*) of the pristine as well as the modified devices under different light wavelengths irradiation (0.98 μW cm^{-2} light intensity and a 2 V bias voltage). R is calculated according to relationship :[1, 32-35]

$$R = \frac{I_{light} - I_{dark}}{PS} \quad (1)$$

where I_{light} is the photocurrent, I_{dark} is the dark current, *S* is the effective light illumination area of the photodetector, and *P* is the light power density. In **Figure 1c**, the PDs showed a higher photoresponse in the UV-vis region than in the near-infrared region. The *R*-value of PVK-Au_NPs-PAI-PDs was 0.1 A W^{-1}, 0.4 A W^{-1}, and 0.03 A W^{-1} at 375 nm, 532 nm, and 808 nm, respectively. Furthermore, the *R* value of PVK-Au_NPs-PAI-PDs was obviously increased compared with the PVK- PDs and PVK-Au_NPs- PDs. The *R* values was increased by four times compared to the PVK-PDs at a light wavelength of 532 nm (**Figure S5a**, Supporting Information). It must be mentioned here that the values of responsivity share a decaying trend with increasing light intensity and finally maintain steady levels, which is probably caused by the

Please cite this paper as: T. Wang, D. Zheng, K. Vegso, G. Baillard, P. Nadazdy, N. Mrkyvkova, P. Siffalovic, Y. Chen, L. Coolen, Th. Pauporte, F. Feng, A Dual Strategy to Enhance the Photoelectric Performance of Perovskite-Based Photodetectors for Application in Optical Communications. Chem. Eng. J. 488 (2024) 151068. https://doi.org/10.1016/j.cej.2024.151068.

intensified carrier recombination rate due to the increased concentration of photocarriers recombination probability at higher light illumination intensity, as well as the presence of defect trap states between the Fermi level and the conduction band edge, which is consistent with previous reports[2, 23, 33].

The specific detectivity, D*, is a figure of merit calculated according to the equation [1,19]:

$$D^* = \frac{R}{\sqrt{\frac{2qI_{dark}}{S}}} \qquad (2)$$

where q is the elementary charge. **Figure S5a** (Supporting Information) shows that D* follows the same trend as R and that the PVK+Au_NPs+PAI-PDs exhibited the best specific detectivity.

We explored the sequential optical switching by measuring the *I-t* curves of both pristine and modified PDs. Only a few switching cycles are shown in **Figure 1e** for reasons of clarity. The on-off switching of the device can be repeated over multiple cycles, demonstrating an effective and stable sequential optical response. Compared to the PVK-PDs, the photocurrent was increased by more than 10 times (14.2 μA) at a 532 nm, a light intensity of 14.77 mW cm^{-2} and a 2 V bias. Furthermore, the I_{light}/I_{dark} current ratios of all devices were characterized at different voltages (**Figure S5b**, Supporting Information). The highest I_{light}/I_{dark} ratio of up to 2.0×10^5 was achieved for PVK-Au_NPs-PAI-PDs at an illumination intensity of 14.77 mW cm^{-2}, which is comparable to published 3D PDs-based perovskite (**Table 1**). **Figure 1f** exhibits the relationship between light intensity and photocurrent for the device. The devices exhibit a wide dynamic range of optical responses between 0.98 μW cm^{-2} and 14.77 mW cm^{-2} (corresponding to a Linear Dynamic Range (LDR) higher than 51 dB as detailed in the Supporting Information).

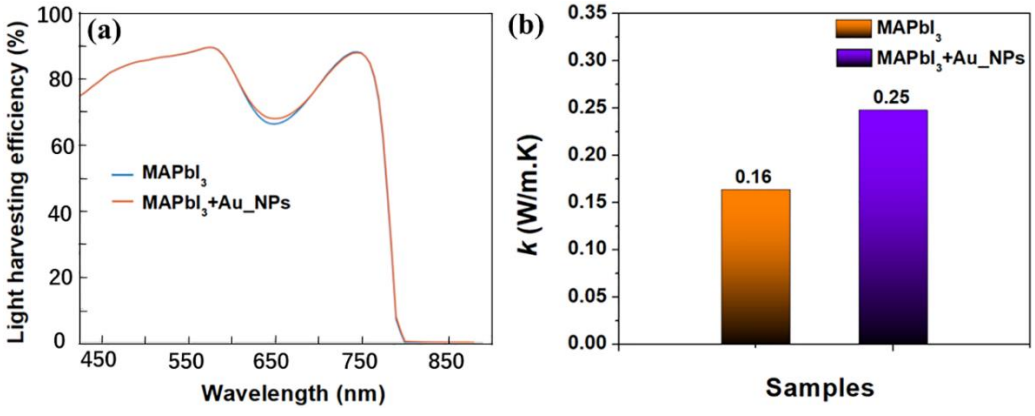

Figure 2. **(a)** Transfer-matrix simulation of light harvesting efficiency for $MAPbI_3$ and

$MAPbI_3$+Au_NPs (Au_NPs volume fraction 0.07%) devices. **(b)** Average thermal conductivity of $MAPbI_3$ and $MAPbI_3$+Au_NPs films.

The measured results confirm that the inclusion of Au_NPs and PAI post-treatment of $MAPbI_3$ perovskite film significantly improves the photoelectric properties. First, for the effect of Au_NPs in the perovskite layer, many reports suggest that it can form localized surface plasmon resonance (LSPR) and higher light absorption caused by light scattering in the perovskite layer, so it can improve the photocurrent of the device [36]. To elucidate this point, the light absorption properties of the film with Au_NPs added were calculated using the transfer matrix method. The average diameter of Au_NPs was 14 nm, as shown in **Figure S2b**. To calculate the light-harvesting efficiency (LHE), we used the transfer-matrix formalism in an effective medium to describe the pristine PD and the PD containing Au_NPs (see **Figure S6**, Supporting Information) [37]. As shown in **Figure 2a**, the results indicate that the LHE spectra of the two samples were similar, with an absorption edge around 780 nm. The film with added Au_NPs exhibited only a slight increase of the absorption at about 640 nm. In addition, due to the low Au_NP volume fraction considered, no significant plasmonic absorption peak was observed due to the LSPR effect.

Despite the fact that the Au_NPs have almost no significant effect on the optical properties of the perovskite layer, they promote better crystallization and reduce defects at grain boundaries, as will be shown below. We studied the thermal conductivity of the pristine and the Au_NPs-added films to elucidate how the introduction of Au_NPs is conducive to better crystallization. As shown in **Figure 2b**, the thermal conductivity of the Au_NPs optimized perovskite film was about 52 % higher compared to the pure perovskite film (see **Table S1** in the Supporting Information). The results indicate that the presence of Au_NPs may lead to more uniform heating of perovskite film during the annealing, thereby helping to improve the crystallinity[38]. **Figure S7** (Supporting Information) shows the Au 4f, I 3d and Pb 4f X-ray photoelectron spectroscopy (XPS) spectra of the perovskite film with and without Au_NPs. The characteristic peak Au 4f and a slight shift to higher binding energy in peak positions of I 3d and Pb 4f can be obviously observed in the $MAPbI_3$+Au_NPs film. Moreover, two small satellite Pb 4f peaks at 136.7 and 141.5 eV around the main ones, corresponding to Pb°, become more obvious after Au doping. XPS spectra indicate a change in chemical valence condition for Pb[31].

Please cite this paper as: T. Wang, D. Zheng, K. Vegso, G. Baillard, P. Nadazdy, N. Mrkyvkova, P. Siffalovic, Y. Chen, L. Coolen, Th. Pauporte, F. Feng, A Dual Strategy to Enhance the Photoelectric Performance of Perovskite-Based Photodetectors for Application in Optical Communications. Chem. Eng. J. 488 (2024) 151068. https://doi.org/10.1016/j.cej.2024.151068.

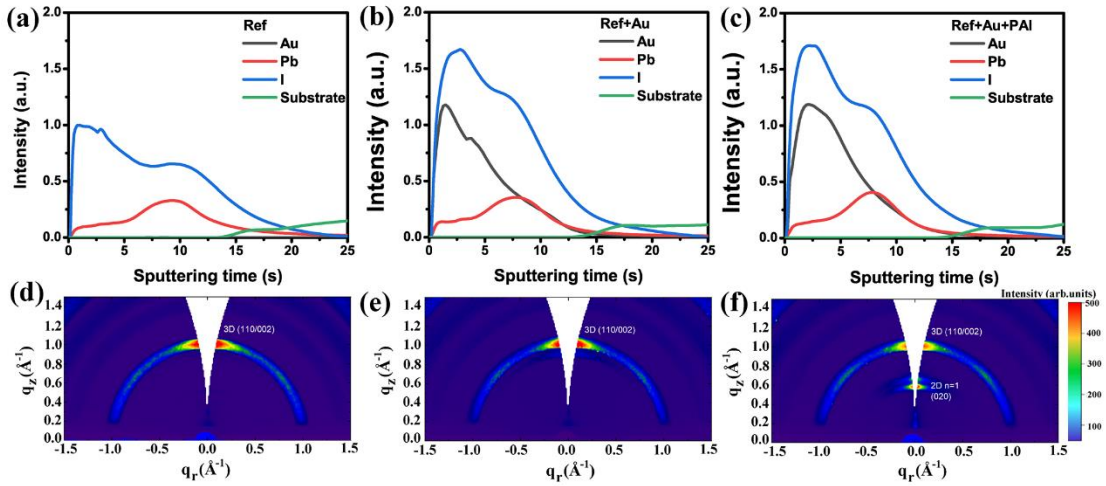

Figure 3. Distribution of main elements determined by GD-OES in **(a)** pure PVK, **(b)** PVK+Au_NPs, and **(c)** PVK+Au_NPs+PAI samples. GIWAXS patterns of **(d)** pure PVK, **(e)** PVK+Au_NPs, and **(f)** PVK+Au_NPs+PAI samples.

To understand the effect of Au_NPs and PAI treatment on the perovskite film formation process, we analyzed the depth profile of the elements in perovskite layers. The element concentrations are reported versus the glow discharge-optical emission spectroscopy (GD-OES) Ar plasma sputtering times in **Figure 3a-c** [4, 39-40]. We measured the depth-resolved element distribution for the pure perovskite, PVK+Au_NPs, and PVK+Au_NPs+PAI films. For reference purposes, the green line represents the substrate. It shows that the substrate was sputtered after about 13-15 s. The time to detect the perovskite layer from the top to the bottom laid between 0 and 12-15 s. The Au distribution in the perovskite film helped us to analyze the recrystallization effect. Au_NPs was observed on the upper part of the perovskite film in **Figure 3b**. It is consistent with our previous work, the detection of changes in the distribution of major elements in the film enabled us to better understand the quality improvement of films [34, 40-41]. In addition, we can conclude that throughout the entire film preparation process, Au_NPs has a positive impact on the surface morphology of the film, as evidenced by the SEM results (**Figure S8,** Supporting Information). After PAI post-treatment (**Figure 3c**), the broadening of the Au distribution (see **Figure 3c**) indicates that the Au_NPs are more evenly dispersed throughout the perovskite layer. The distribution of Au after PAI post-treatment becomes more uniform because PAI solution promotes a recrystallization effect on the whole film, which is not limited to the surface but affect the entire film, and the degree of recrystallization decreases from top to bottom. At the same time, when PAI solution also has a certain solubility to perovskite film, Au enriched in the upper layer will move more deeply into the film with a downward permeation. Moreover, the gold curve's peak right-shift, indicating that the capping layer formed by the recrystallization of PAI effectively covers most of

the gold particles (see **Note 3** and **Figure S8,** Supporting Information). The crystal structure and texture of perovskite were further studied with grazing-incidence wide-angle X-ray scattering (GIWAXS), as shown in **Figure 3d-f**. $MAPbI_3$ perovskite crystallizes in the tetragonal space group (I4/mcm). Using lattice parameters indices determined through X-ray diffraction to index GIWAXS patterns[42-43]. The azimuthal spread of the 110/002 diffraction spot of the 3D perovskite confirms a uniaxial texture. The same is applicable for 2D PAI-based perovskite, based on the similar azimuthal spread of the 020 diffraction spot, it confirms the uniaxial texture parallel to the (010) lattice plane of the substrate (**Figure 3f**). Furthermore, from the position of 020 diffraction ($q_z = 0.58$ Å^{-1}) of the 2D perovskite, we can assume that the $(PA)_2PbI_4$ (n=1) 2D perovskite layer was formed after PAI treatment. This is further corroborated by a distinct shoulder in the absorption spectrum (at ca. 500 nm) matching the absorption peak of $(PA)_2PbI_4$ (n=1) 2D perovskite (**Figure S9a,** Supporting Information). The small diffraction spot at $q_z = 0.66$ Å^{-1} can be assigned to the decomposition of 2D to 0D crystals[44]. The introduction of Au_NPs into the perovskite layer during recrystallization with PAI also had no detrimental effect on the crystalline texture since the GIWAXS pattern remained unchanged (**Figure 3e**). This indicates that Au_NPs may have undergone segregation at the grain boundaries. The enhanced perovskite structure can serve as an efficient charge transport channel, achieving high-efficiency charge transport and extraction, which is helpful in improving the photoelectric performance of the PDs.

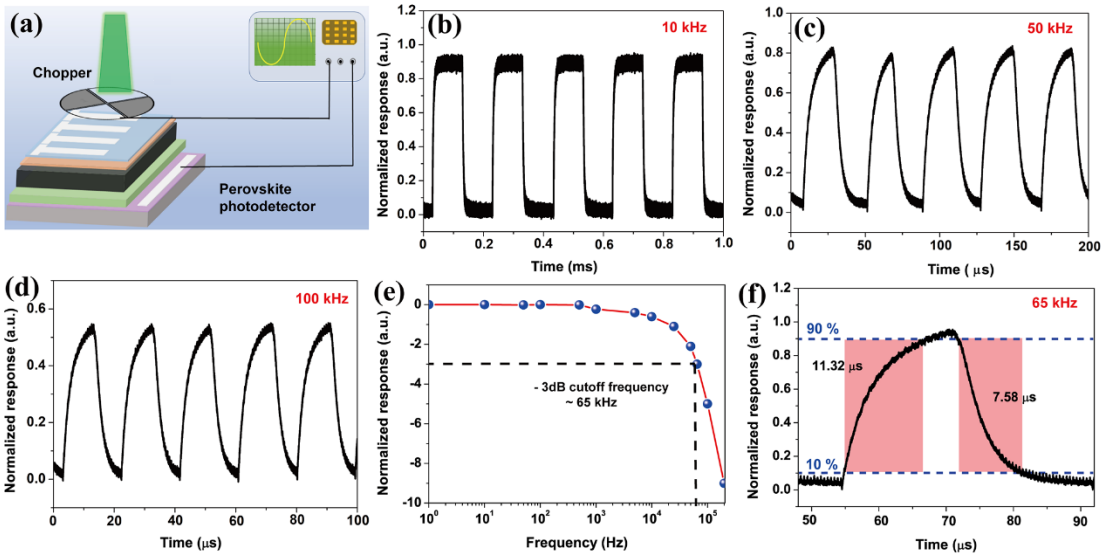

Figure 4. (a) Schematic diagram of the experimental equipment for measuring the PDs photoresponse speed. **(b-d)** The temporal optical response of the PDs under the irradiation of square wave light signal of different frequencies. **(e)** The relationship between photoresponse and input

frequency is normalized to estimate the 3 dB cut-off frequency of the PDs. **(f)** A single light response curve at 65 kHz.

Perovskite optoelectronic devices have potential application prospects in the field of optical communication, especially in optical signal receivers with high-speed photoelectric response in the visible range. Therefore, the response time of PVK-Au_NPs-PAI-PDs at different optical signal frequencies was studied. The light beam from a 532 nm laser was modulated by an optical chopper controlled by a function generator to produce a square wave optical signal (**Figure 4a)**. **Figure 4b-c** and **Figure S10** show that the device signal was stable and reproducible over a wide range of frequencies. By using the relationship between normalized photoresponse and modulation frequency (**Figure 4e**), the 3 dB cut-off frequency ($f_{\text{-3dB}}$) was determined at 65 kHz, almost of the same order of magnitude as the reported photodiode of $MAPbI_3$, which is sufficient for efficient data receiver application [33]. On the single photoresponse curve of 65 kHz (**Figure 4f**), the response time of the device τ_{rise} and τ_{fall} are determined at 11.32 and 7.58 μs, respectively. In general, the responsivity and photoresponse speed of our device are better than the reported values from previous works, as summarized in **Table 1**. This excellent performance is mainly related to the combination of enhanced charge transport and inhibition recombination in our devices.

Please cite this paper as: T. Wang, D. Zheng, K. Vegso, G. Baillard, P. Nadazdy, N. Mrkyvkova, P. Siffalovic, Y. Chen, L. Coolen, Th. Pauporte, F. Feng, A Dual Strategy to Enhance the Photoelectric Performance of Perovskite-Based Photodetectors for Application in Optical Communications. Chem. Eng. J. 488 (2024) 151068. https://doi.org/10.1016/j.cej.2024.151068.

Table 1. Comparison of the performance parameters of 3D metal lead halide perovskite-based PDs.

Device structure	R [A W^{-1}] (Bias, wavelength, irradiance)	D* [Jones]	Photocurrent	Rising/ falling time	On/off	cut-off frequency	Wavelength	Stability test time	Ref.
(Vertical) Ag/BCP/PCBM/$MAPbI_3$:CuSCN/ITO	0.37 (0 V, 685 nm, --)	1.06×10^{12}	2.4 mA	5.02/5.50 µs	----	50 kHz	350-750 nm	>3000 s	[33]
(Vertical) Ag/P3HT/$MAPbI_3$/PCBM/ TiO_2/$MAPbBr_3$/P3HT/NiO_x/ITO	0.046(0.7 V, 710 nm, 0.01 W cm^{-2})	1.75×10^{10}	2 mA	----	7.8×10^{7}	33 kHz	300-800 nm	----	[47]
(Lateral) In/GaN-$Cs_2AgBiBr_6$/Ag	1.46 (0 V, 265 nm, 0.005 mW cm^{-2})	9.4×10^{12}	10^{-4} A	3.4/8.4 ms	10^4	----	265 nm	>100days	[35]
(Vertical) Au/PEDOT:PSS/ $MAPbI_3$ film/PCBM/Al	0.314 (0 V, 670 nm, 1 mW cm^{-2})	----	----	4.0 /3.3 µs	10^4	30 kHz	400-750 nm	----	[48]
(Lateral) Au/2D $FAPbI_3$/Au	3.27 (9 V, 645 nm,18 nW cm^{-2})	1.35×10^{12}	800 nA	0.3/0.5 ms	----	----	<815 nm	>1400 s	[49]
(Lateral) Au/$MAPbI_3$ arrays/Au	0.1 (10 V, 650 nm,100 µW cm^{-2})	1.02×10^{12}	20 nA	0.3 ms/0.4 ms	300	----	<800 nm	4 weeks	[50]
(Vertical) Al/BCP/C60/PCBM/ $MAPbI_3$ Poly/PEDOT:PSS/ITO	0.21 (-2 V, white light, 143 µW cm^{-2})	7.4×10^{12}	----	120 ns	----	3500 Hz	<800 nm	45 days	[25]
(Vertical) Au/PTAA/ $MAPbI_3$/ Au nanosquares/Au	----	7.13×10^{11}	58 nA	----	----	----	600-900 nm	>120 h	[51]
(Lateral) Au/ C8BTBT-$MAPbI_3$/Au	24.8 (10 V, 532 nm, 0.37 mW cm^{-2})	7.7×10^{12}	28.7 µA	4.0/5.8 ms	2.4×10^4	----	300-850 nm	>20 days	[52]
(Lateral) Si/SiO_2/Au/$MAPbI_3$/Au/SiO_2/Si	0.018(-2 V, 970 nm, 0.05 mW cm^{-2})	1.8×10^{12}	8 nA	----	298	----	400-1200 nm	----	[53]
(Vertical) ITO/PTAA:F4-TCNQ/ $MAPbI_3$: Au_NPs/PCBM/BCP/Au	0.4 (2 V, 532 nm, 0.98 µW cm^{-2})	3.6×10^{11}	14 µA	11.3/7.5 µs	2.0×10^5	65 kHz	405-808 nm	>100 days	This work

The environmental stability of PDs based on 3D perovskite is a key issue that needs to be addressed. We examined the long-term stability of the PDs' photoelectric performance (**Figure S11**). The unencapsulated samples were stored at ambient conditions. The photocurrent of the $MAPbI_3$ PDs exhibited very low stability, decreasing from 1.4 μA to 0.001 μA within 5 days. The degradation trend of PVK+Au_NPs-PDs was almost the same as that of PVK-PDs. In contrast, the photocurrent of PVK+Au_NPs+PAI-PDs remained almost the same over 100 days, decreasing from 14 μA to only 12.5 μA. Compared with PVK-PDs, the modified PVK+Au_NPs+PAI-PDs exhibit outstanding environmental stability due to the PAI post-treatment of the perovskite film, which is due to the formation of a quasi-2D perovskite capping layer on the $MAPbI_3$ perovskite layer top surface. The quasi-2D $(PA)_2PbI_4$ (n=1) perovskite capping layer forms a protective barrier, which protects the underlying 3D $MAPbI_3$ perovskite film from degradation and reduces charge recombination, enhancing the photoelectric performance of the device. Thus, PDs with high photoresponsivity and better ambient stability can provide significant advantages for the widespread applications of optical communications and imaging sensors[1, 47, 54].

To show that the modified-PDs structure can produce better photoelectric performance, we studied the energy band structure of the device (**Figures 5a,b**). Ultraviolet electron spectroscopy (UPS) was used to analyze the energy band arrangement using a monochromatic He excitation source at hν= 21.22 eV. The valence band maximum (E_{VBM}) and the conduction band minimum (E_{CBM}) energy levels of perovskite film are shown in **Figure 5a**. The work function was 4.7 eV, and the calculated difference between E_F and E_{VBM} was 0.7 eV. We measured the $MAPbI_3$ band gap at 1.60 eV (**Figure S3a**). With the energy level matching in the device, as shown in **Figure 5b**, photogenerated carriers were quickly extracted to achieve high responsivity of devices. **Figure 5c** shows the time-resolved PL (TRPL) spectra based on the glass/perovskite structure, measured under 470 nm laser excitation. TRPL is an effective method for detecting the trap states in the perovskite[44, 55]. The increased lifetime for the modified perovskite structures indicates passivation of the grain boundaries of perovskite films, resulting in a reduced density of trapped states. In other words, using Au_NPs and PAI recrystallization process results in better crystal quality with fewer defects. Moreover, Au_NPs can increase the charge transfer pathway and suppress the photoinduced electron-hole pair recombination[56]. Accordingly, this was the primary mechanism for increasing the lifetime of the modified perovskite structure. This unique structure can not only reduce defects state density and grain boundaries of film but also reduce interface recombination, thereby increasing the photocurrent of the device. This was a key factor in the preparation of high-performance heterojunction PDs.

Please cite this paper as: T. Wang, D. Zheng, K. Vegso, G. Baillard, P. Nadazdy, N. Mrkyvkova, P. Siffalovic, Y. Chen, L. Coolen, Th. Pauporte, F. Feng, A Dual Strategy to Enhance the Photoelectric Performance of Perovskite-Based Photodetectors for Application in Optical Communications. Chem. Eng. J. 488 (2024) 151068. https://doi.org/10.1016/j.cej.2024.151068.

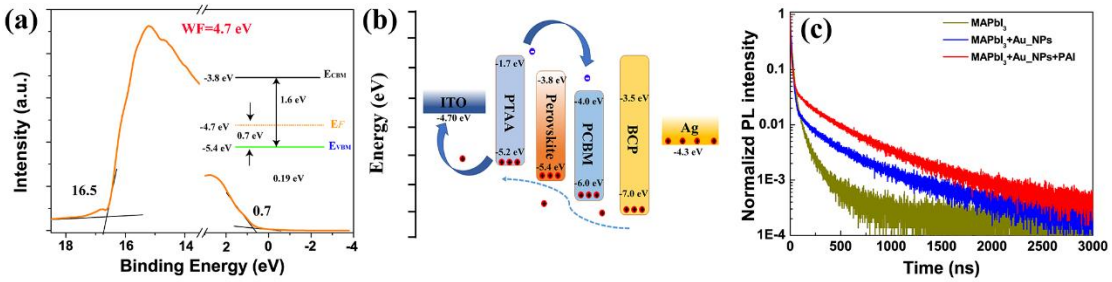

Figure 5. (a) UPS soectrum of PVK+Au_NPs+PAI film. Deduced work function and energy difference between the Fermi level (E_F) and valence band maximum (E_{VBM}) of perovskite. **(b)** Energy level diagram and hole-electron transfer in the device. **(c)** Time-resolved PL curve of pristine and modified perovskite films.

We integrated the PDs as an optical signal receiver into a visible light communication system (**Figure 6**). The advantages of visible light communication are its low energy consumption, high-speed operation, and strong anti-interference ability[35, 47, 55]. Information transmission through high-speed optical pulse signals, combining lighting communication and control functions, has a wide range of applications in intelligent transportation, smart homes, high-speed audio transmission, and other fields[2-3, 45]. The visible light communication system is mainly composed of two parts: a transmitter and a receiver, where the transmitter is used to drives the LED, and the receiver processes the signal. The visible light communication system structure schematic diagram is shown in **Figure 6a**. The driver converts computer date into analog signals 1 and 0, corresponding to the high levels and low voltage levels, respectively. By modulating the light output of LED and illuminating PDs to generate high and low photocurrent. Next, convert it into a voltage signal and transmit it to another driver so that the voltage signal is converted into digital data. To better illustrate the data transmission process, the string "MAPbI3" is encoded by ASCII (American Standard Code for Information Interchange). The high light intensity is represented by "1", and the low light intensity is represented by "0". By transmitting the optical signal to PDs, electrical signals are read with high and low levels. Finally, the electrical signal is demodulated to a " $MAPbI_3$" string (**Figure 6b**). Due to the fast response speed of PDs (**Figure 4f**), even if the coding frequency is changed, the encoding process is not affected (**Figure S12**, Supporting information). As shown in **Figure 6c**, the current signals that the device can receive modulated optical information at different bit rates, indicating that the system can transmit data at bit rates up to 200 kbps. Based on the actual response speed of the measured PDs, they are capable of transmitting a bit rate of 1 Mbps or higher. However, the bandwidth limitation of the preamplifier can affect the actual transmission rate of the device. In general, this study shows that our PDs can be used for optical communication.

Please cite this paper as: T. Wang, D. Zheng, K. Vegso, G. Baillard, P. Nadazdy, N. Mrkyvkova, P. Siffalovic, Y. Chen, L. Coolen, Th. Pauporte, F. Feng, A Dual Strategy to Enhance the Photoelectric Performance of Perovskite-Based Photodetectors for Application in Optical Communications. Chem. Eng. J. 488 (2024) 151068. https://doi.org/10.1016/j.cej.2024.151068.

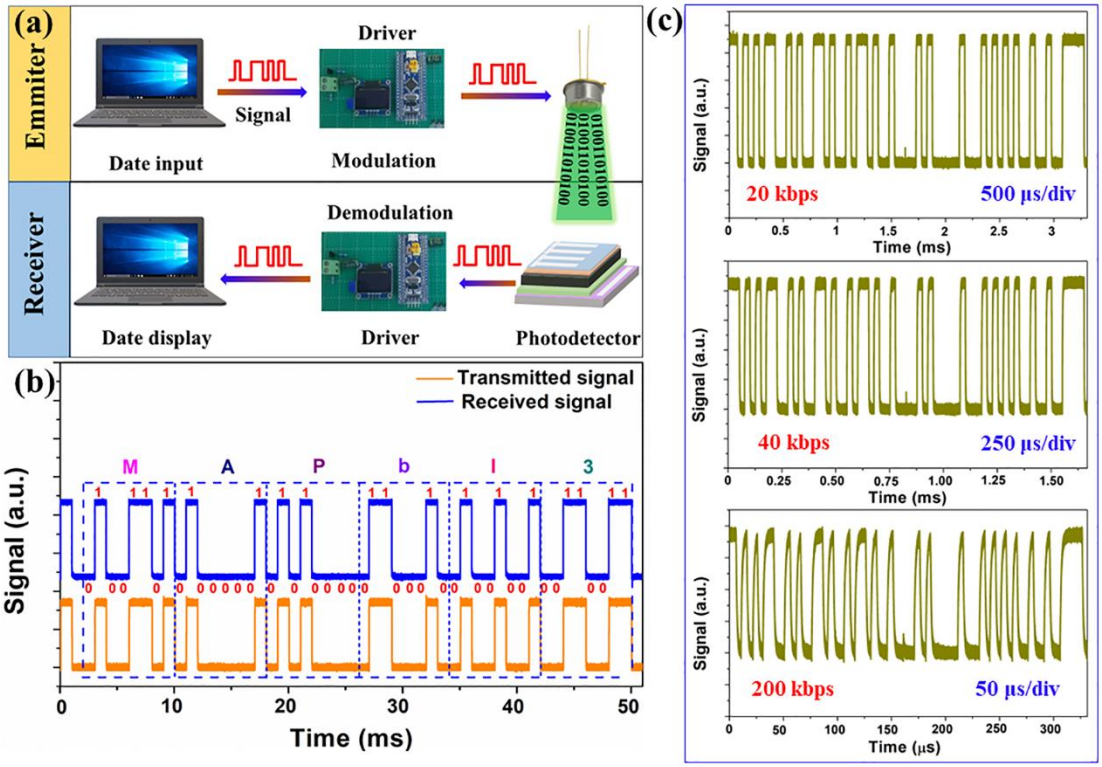

Figure 6. (a) Visible light communication system structure schematic diagram. **(b)** Electrical signal waveform obtained from single-chip processor and PDs. **(c)** Digital data waveform received by devices with different transmission rates.

Conclusions

In summary, we have prepared high-quality $MAPbI_3$ perovskite films using sputtered Au_NPs and PAI recrystallization, which decreased the grain boundaries and defects, and improved environmental stability. The device exhibited a high responsivity of 0.4 A W^{-1}, an on/off current ratio of 2.0 × 10^5, and response times of 11.3 μs /7.58 μs, which is a significant improvement of the performance over the pristine PDs. In addition, the modified PDs exhibited excellent environmental stability (100 days) under ambient conditions without encapsulation. Finally, the PDs were integrated into a visible light communication system and successfully served as optical signal receivers to transmit ASCII-encoded information. The research results indicate that stable and high-speed perovskite PDs with a p-i-n structure have great potential applications in the field of optical communications.

Please cite this paper as: T. Wang, D. Zheng, K. Vegso, G. Baillard, P. Nadazdy, N. Mrkyvkova, P. Siffalovic, Y. Chen, L. Coolen, Th. Pauporte, F. Feng, A Dual Strategy to Enhance the Photoelectric Performance of Perovskite-Based Photodetectors for Application in Optical Communications. Chem. Eng. J. 488 (2024) 151068. https://doi.org/10.1016/j.cej.2024.151068.

Experimental Section

Materials

Lead iodide (PbI_2, 99.99%), methylamine iodide (MAI, 99.5%), propylammonium iodide (PAI, 99.5%) were purchased from Xi'an Polymer Light Technology Corp. [6,6]-phenyl-C61-butyric acid methyl ester (PCBM, 99.9%) and bathocuproine (BCP, 99.5%) molecules were purchased from Advanced Election Technology Co., Ltd. Dimethyl sulfoxide (DMSO, GC, 99.9%), isopropanol (C_3H_8O, AR, 99%), chlorobenzene (C_6H_5Cl, AR, 99%) and methylbenzene (C_7H_8, AR, ≥99.5%) were purchased from Aladdin Chemical Reagent Co., Ltd. The ITO substrate was purchased from Liaoning Preferred New Energy Technology Co. Ltd.

Device Fabrication

First, the ITO substrates were cleaned by irradiation with UV ozone for 20 min. In a N_2 filled glovebox a PTAA:F4-TCNQ solution (14.4 mg PTAA and 1.6 mg F4-TCNQ in 2 mL toluene) was spin-coated onto the ITO substrates at 3000 rpm for 30 s, and then annealed at 150 ℃ for 20 min. The $MAPbI_3$ precursor solution was prepared by dissolving 668.5 mg PbI_2 and 230.5 mg MAI in 1 mL DMSO. This solution was stirred at 60 ℃ for 2 h. The film was then prepared by spin-coating at 1000 rpm for 10 s and 4000 rpm for 30 s, then 100 μL of chlorobenzene was dripped 30 s after the spin-coating began. The layer was annealed at 100 ℃ for 30 s. Next, Au_NPs were immediately sputtered on the surface of the perovskite layer using an ion sputter coater SuPro Instrument ISC150 operated at 10 W. The optimized sputtering time was 15s. Finally, the layers were annealed on a hotplate at 100 ℃ for 60 min. Subsequently, a PAI solution was spin-coated at 3000 rpm for 20 s. The PCBM was spin-coated at 2000 rpm for 30 s. The BCP was spin-coated at 4000 rpm for 30 s. Both were heated at 100 ℃ for 15 min. Finally, a Cr/Ag electrodes with a thickness of 10 nm/100 nm, respectively, were evaporated through a shadow mask using a high-vacuum e-beam evaporator. The full device preparation process is summarized in **Figure S1** (Supporting Information).

Characterizations and Measurements

The morphology of perovskite films was examined using SEM (GeminiSEM 560, 2 kV acceleration voltage). XRD data were measured by a high-resolution diffractometer with Cu Kα source radiation (3 kW, 40 mA, λ = 0.154 nm). The UV-vis absorption spectra were obtained on a PerkinElmer spectrophotometer (LAMBDA). The PL spectra were acquired at 10 nW excitation power using a 488-nm long-pass filter. The time-resolved PL attenuation on the glass substrate was analyzed. The perovskite was excited with a 470 nm diode laser. The ultraviolet photoelectron spectrometer (UPS)

was measured by a ThermoFisher Nexsa using a monochromatic He excitation source at hν= 21.22 eV. The GIWAXS patterns were measured using a microfocus X-ray source (IμS, Incoatec, Germany) and a single-photon counting 2D X-ray detector (Pilatus 100 K, Dectris, Switzerland). For GD-OES characterizations, the argon plasma was generated by applying a power of 17W at an argon pressure of 420 Pa. The perovskite film was installed on the O-ring on one side of the plasma chamber to serve as the cathode. The photoelectric properties of the PDs were measured with a Keithley 2614 B electrometer. PD measurements were carried out using a laser diode as a light source.

Transfer-matrix simulation

The optical modeling was carried out in the form of the transfer-matrix. The effective-medium was approximated for the perovskite layer with Au_NPs, and the Maxwell-Garnett equation was used to treat the effective index of the film medium. The dielectric constant of the gold was acquired by Johnson and Christy, while the refractive index of perovskite was obtained from the literature[58].

Acknowledgments

This work was supported by the grant SAS-MOST/JRP/2021/192/PB-free-PSC, Center-initiated research project of Zhejianglab (No. 113014-AL2209), the National Natural Science Foundation of China (grant No. 62204069 and No. 62275167), the Shenzhen Fundamental research project (grant No. JCYJ20210324120402006, JCYJ20210324131206018, RCYX20221008092847060, and GXWD20220811163751003), the GuangDong Basic and Applied Basic Research Foundation (grant No. 2022A1515011464, No. 2023B1515020032, and No. 2020A1515010598), the National Key Research and Development Program of China (grant No. 2023YFB2806700), the Key Research and Development Program of Guangdong Province (grant No. 2023B0101200009), and the Fundamental Research Funds for the Central Universities (HIT.OCEF.2023023).

References

1. Bao, C.; Yang, J.; Bai, S.; Xu, W.; Yan, Z.; Xu, Q.; Liu, J.; Zhang, W.; Gao, F., High Performance and Stable All-Inorganic Metal Halide Perovskite-Based Photodetectors for Optical Communication Applications. *Adv Mater* **2018,** *30* (38), e1803422.

2. Cen, G.; Liu, Y.; Zhao, C.; Wang, G.; Fu, Y.; Yan, G.; Yuan, Y.; Su, C.; Zhao, Z.; Mai, W., Atomic-Layer Deposition-Assisted Double-Side Interfacial Engineering for High-Performance Flexible and Stable $CsPbBr_3$ Perovskite Photodetectors toward Visible Light Communication Applications. *Small* **2019,** *15* (36), e1902135.

3. Kang, C. H.; Dursun, I.; Liu, G.; Sinatra, L.; Sun, X.; Kong, M.; Pan, J.; Maity, P.; Ooi, E. N.; Ng, T. K.; Mohammed, O. F.; Bakr, O. M.; Ooi, B. S., High-speed colour-

converting photodetector with all-inorganic $CsPbBr_3$ perovskite nanocrystals for ultraviolet light communication. *Light Sci Appl* **2019,** *8*, 94.

4. Wang, T.; Zheng, D.; Vegso, K.; Mrkyvkova, N.; Siffalovic, P.; Yuan, X.; Somekh, M. G.; Coolen, L.; Pauporte, T.; Fu, F., Flexible Array of High Performance and Stable Formamidium-Based Low-n 2D Halide Perovskite Photodetectors for Optical Imaging. *Nano Energy* **2023**, *116*, 108827.

5. Wang, T.; Zheng, D.; Vegso, K.; Mrkyvkova, N.; Siffalovic, P.; Pauporté, T., High-Resolution and Stable Ruddlesden–Popper Quasi-2D Perovskite Flexible Photodetectors Arrays for Potential Applications as Optical Image Sensor. *Advanced Functional Materials* **2023**, *33*(43), 2304659.

6. Lin, K. T.; Chen, H. L.; Lai, Y. S.; Yu, C. C., Silicon-based broadband antenna for high responsivity and polarization-insensitive photodetection at telecommunication wavelengths. *Nat Commun* **2014,** *5*, 3288.

7. Pan, X.; Zhang, J.; Zhou, H.; Liu, R.; Wu, D.; Wang, R.; Shen, L.; Tao, L.; Zhang, J.; Wang, H., Single-Layer ZnO Hollow Hemispheres Enable High-Performance Self-Powered Perovskite Photodetector for Optical Communication. *Nanomicro Lett* **2021,** *13* (1), 70.

8. Li, C.; Lu, J.; Zhao, Y.; Sun, L.; Wang, G.; Ma, Y.; Zhang, S.; Zhou, J.; Shen, L.; Huang, W., Highly Sensitive, Fast Response Perovskite Photodetectors Demonstrated in Weak Light Detection Circuit and Visible Light Communication System. *Small* **2019,** *15* (44), e1903599.

9. Jang, J.; Park, Y. G.; Cha, E.; Ji, S.; Hwang, H.; Kim, G. G.; Jin, J.; Park, J. U., 3D Heterogeneous Device Arrays for Multiplexed Sensing Platforms Using Transfer of Perovskites. *Adv Mater* **2021,** *33* (30), e2101093.

10. Chen, J.; Priya, A. S.; You, D.; Pei, W.; Zhang, Q.; Lu, Y.; Li, M.; Guo, J.; He, Y., Self-driven ultraviolet photodetectors based on ferroelectric depolarization field and interfacial potential. *Sensors and Actuators A: Physical* **2020,** *315*, 112267.

11. Guo, J.; Liu, Y.; Lin, Y.; Tian, Y.; Zhang, J.; Gong, T.; Cheng, T.; Huang, W.; Zhang, X., Simulation of tuning graphene plasmonic behaviors by ferroelectric domains for self-driven infrared photodetector applications. *Nanoscale* **2019,** *11* (43), 20868-20875.

12. Zou, Z.; Liang, J.; Zhang, X.; Ma, C.; Xu, P.; Yang, X.; Zeng, Z.; Sun, X.; Zhu, C.; Liang, D.; Zhuang, X.; Li, D.; Pan, A., Liquid-Metal-Assisted Growth of Vertical GaSe/MoS_2 p-n Heterojunctions for Sensitive Self-Driven Photodetectors. *ACS Nano* **2021,** *15* (6), 10039-10047.

13. Song, W.; Chen, J.; Li, Z.; Fang, X., Self-Powered MXene/GaN van der Waals Heterojunction Ultraviolet Photodiodes with Superhigh Efficiency and Stable Current Outputs. *Adv Mater* **2021,** *33* (27), e2101059.

14. Zhu, T.; Su, J.; Alvarez, J.; Lefèvre, G.; Labat, F.; Ciofini, I.; Pauporté, T., Response Enhancement of Self-Powered Visible-Blind UV Photodetectors by Nanostructured Heterointerface Engineering. *Advanced Functional Materials* **2019,** *29* (38), 1903981.

15. Zhu, H.; Fu, Y.; Meng, F.; Wu, X.; Gong, Z.; Ding, Q.; Gustafsson, M. V.; Trinh, M. T.; Jin, S.; Zhu, X. Y., Lead halide perovskite nanowire lasers with low lasing thresholds and high quality factors. *Nat Mater* **2015,** *14* (6), 636-42.

16. Cao, F.; Hu, Z.; Yan, T.; Hong, E.; Deng, X.; Wu, L.; Fang, X., A Dual-Functional Perovskite-Based Photodetector and Memristor for Visual Memory. *Adv Mater* **2023,** *35* (44), e2304550.
17. Cao, F.; Li, Z.; Liu, X.; Shi, Z.; Fang, X., Air Induced Formation of $Cs_3Bi_2Br_9/Cs_3BiBr_6$ Bulk Heterojunction and Its Dual-band Photodetection Abilities for Light Communication. *Advanced Functional Materials* **2022,** *32* (46), 2206151.
18. Yan, T.; Li, Z.; Su, L.; Wu, L.; Fang, X., Bidirectional and Dual-Mode Organic Photodetector Enables Secure Ultraviolet Communication. *Advanced Functional Materials* **2023,** *33* (31), 2302746.
19. Zheng, D.; Pauporté, T., Advances in Optical Imaging and Optical Communications Based on High-Quality Halide Perovskite Photodetectors. *Advanced Functional Materials* **2023**, 2311205.
20. Wang, W.; Jiang, H.; Li, L.; Li, G., Two-dimensional group-III nitrides and devices: a critical review. *Rep Prog Phys* **2021,** *84* (8), 086501.
21. Lin, Z.; Lin, T.; Lin, T.; Tang, X.; Chen, G.; Xiao, J.; Wang, H.; Wang, W.; Li, G., Ultrafast response self-powered UV photodetectors based on GaS/GaN heterojunctions. *Applied Physics Letters* **2023,** *122* (13), 131101.
22. Ban, M.; Zou, Y.; Rivett, J. P. H.; Yang, Y.; Thomas, T. H.; Tan, Y.; Song, T.; Gao, X.; Credgington, D.; Deschler, F.; Sirringhaus, H.; Sun, B., Solution-processed perovskite light emitting diodes with efficiency exceeding 15% through additive-controlled nanostructure tailoring. *Nat Commun* **2018,** *9* (1), 3892.
23. Li, Y.; Shi, Z.; Lei, L.; Zhang, F.; Ma, Z.; Wu, D.; Xu, T.; Tian, Y.; Zhang, Y.; Du, G.; Shan, C.; Li, X., Highly Stable Perovskite Photodetector Based on Vapor-Processed Micrometer-Scale $CsPbBr_3$ Microplatelets. *Chemistry of Materials* **2018,** *30* (19), 6744-6755.
24. Pan, R.; Li, H.; Wang, J.; Jin, X.; Li, Q.; Wu, Z.; Gou, J.; Jiang, Y.; Song, Y., High-Responsivity Photodetectors Based on Formamidinium Lead Halide Perovskite Quantum Dot-Graphene Hybrid. *Particle & Particle Systems Characterization* **2018,** *35* (4), 1700304.
25. Fang, Y.; Huang, J., Resolving Weak Light of Sub-picowatt per Square Centimeter by Hybrid Perovskite Photodetectors Enabled by Noise Reduction. *Adv Mater* **2015,** *27* (17), 2804-10.
26. Fang, C.; Wang, H.; Shen, Z.; Shen, H.; Wang, S.; Ma, J.; Wang, J.; Luo, H.; Li, D., High-Performance Photodetectors Based on Lead-Free 2D Ruddlesden-Popper Perovskite/MoS_2 Heterostructures. *ACS Appl Mater Interfaces* **2019,** *11* (8), 8419-8427.
27. Ji, T.; Zhang, H.; Han, N.; Wang, W.; Wu, B.; Li, G.; Fan, M.; Li, Z.; Hao, Y.; Zhu, F.; Wu, Y.; Cui, Y., Plasmonic nanoprism enhanced quasi-2D Ruddlesden-Popper layered perovskite photodetectors. *Journal of Materials Chemistry C* **2020,** *8* (3), 1110-1117.
28. Shi, Z.; Li, Y.; Li, S.; Li, X.; Wu, D.; Xu, T.; Tian, Y.; Chen, Y.; Zhang, Y.; Zhang, B.; Shan, C.; Du, G., Localized Surface Plasmon Enhanced All-Inorganic Perovskite Quantum Dot Light-Emitting Diodes Based on Coaxial Core/Shell Heterojunction Architecture. *Advanced Functional Materials* **2018,** *28* (20), 1707031.

29. Wang, F.; Zou, X.; Xu, M.; Wang, H.; Wang, H.; Guo, H.; Guo, J.; Wang, P.; Peng, M.; Wang, Z.; Wang, Y.; Miao, J.; Chen, F.; Wang, J.; Chen, X.; Pan, A.; Shan, C.; Liao, L.; Hu, W., Recent Progress on Electrical and Optical Manipulations of Perovskite Photodetectors. *Advanced Science* **2021,** *8* (14), 2100569.

30. Zheng, D.; Pauporté, T.; Schwob, C.; Coolen, L., Models of light absorption enhancement in perovskite solar cells by plasmonic nanoparticles. *Exploration* **2023,** *4* (1), 20220146.

31. Li, Z.; Yan, T.; Fang, X., Low-dimensional wide-bandgap semiconductors for UV photodetectors. *Nature Reviews Materials* **2023,** *8* (9), 587-603.

32. Chen, Y.; Su, L.; Jiang, M.; Fang, X., Switch type PANI/ZnO core-shell microwire heterojunction for UV photodetection. *Journal of Materials Science & Technology* **2022,** *105*, 259-265.

33. Liu, Z.; Liu, X.; Sun, B.; Tan, X.; Ye, H.; Zhou, J.; Tang, Z.; Shi, T.; Liao, G., A Cu-Doping Strategy to Enhance Photoelectric Performance of Self-Powered Hole-Conductor-Free Perovskite Photodetector for Optical Communication Applications. *Advanced Materials Technologies* **2020,** *5* (8), 2000260.

34. Chen, S.; Teng, C.; Zhang, M.; Li, Y.; Xie, D.; Shi, G., A Flexible UV-Vis-NIR Photodetector based on a Perovskite/Conjugated-Polymer Composite. *Adv Mater* **2016,** *28* (28), 5969-74.

35. Li, Y.; Shi, Z.; Lei, L.; Li, S.; Yang, D.; Wu, D.; Xu, T.; Tian, Y.; Lu, Y.; Wang, Y.; Zhang, L.; Li, X.; Zhang, Y.; Du, G.; Shan, C., Ultrastable Lead-Free Double Perovskite Photodetectors with Imaging Capability. *Advanced Materials Interfaces* **2019,** *6* (10), 1900188.

36. Zheng, D.; Schwob, C.; Prado, Y.; Ouzit, Z.; Coolen, L.; Pauporté, T., How do gold nanoparticles boost the performance of perovskite solar cells? *Nano Energy* **2022,** *94*, 106934.

37. Wang, T.; Zheng, D.; Zhang, J.; Qiao, J.; Min, C.; Yuan, X.; Somekh, M.; Feng, F., High-Performance and Stable Plasmonic-Functionalized Formamidinium-Based Quasi-2D Perovskite Photodetector for Potential Application in Optical Communication. *Advanced Functional Materials* **2022**, *32*(48), 2208694.

38. Sun, Z.; Aigouy, L.; Chen, Z., Plasmonic-enhanced perovskite-graphene hybrid photodetectors. *Nanoscale* **2016,** *8* (14), 7377-7383.

39. Ma, C.; Zheng, D.; Demaille, D.; Gallas, B.; Schwob, C.; Pauporté, T.; Coolen, L., Light management in highly-textured perovskite solar cells: From full-device ellipsometry characterization to optical modelling for quantum efficiency optimization. *Solar Energy Materials and Solar Cells* **2021,** *230*, 111144.

40. Lee, Y. H.; Park, S.; Won, Y.; Mun, J.; Ha, J. H.; Lee, J. H.; Lee, S. H.; Park, J.; Yeom, J.; Rho, J.; Ko, H.; Oh, J. H., Flexible high-performance graphene hybrid photodetectors functionalized with gold nanostars and perovskites. *NPG Asia Materials* **2020,** *12* (1), 1-12.

41. Zheng, D.; Volovitch, P.; Pauporté, T., What Can Glow Discharge Optical Emission Spectroscopy (GD-OES) Technique Tell Us about Perovskite Solar Cells? *Small Methods* **2022,** *6* (11), 2200633.

42. Zheng, D.; Raffin, F.; Volovitch, P.; Pauporte, T., Control of perovskite film crystallization and growth direction to target homogeneous monolithic structures. *Nat Commun* **2022,** *13* (1), 6655.

43. Zheng, D.; Zhu, T.; Yan, Y.; Pauporté, T., Controlling the Formation Process of Methylammonium-Free Halide Perovskite Films for a Homogeneous Incorporation of Alkali Metal Cations Beneficial to Solar Cell Performance. *Advanced Energy Materials* **2022,** *12* (13), 2103618.

44. Wang, T.; Hou, S.; Zhang, H.; Yang, Y.; Xu, W.; Ao, T.; Kang, M.; Pan, G.; Mao, Y., Highly controllable synthesis of $MAPbI_3$ perovskite nanocrystals with long carrier lifetimes and narrow band gap for application in photodetectors. *Journal of Alloys and Compounds* **2021,** *872*, 159589.

45. Gao, D.; Li, R.; Chen, X.; Chen, C.; Wang, C.; Zhang, B.; Li, M.; Shang, X.; Yu, X.; Gong, S.; Pauporté, T.; Yang, H.; Ding, L.; Tang, J.; Chen, J., Managing Interfacial Defects and Carriers by Synergistic Modulation of Functional Groups and Spatial Conformation for High-Performance Perovskite Photovoltaics Based on Vacuum Flash Method. *Advanced Materials* **2023,** *35* (23), 2301028.

46. Vasileiadou, E. S.; Jiang, X.; Kepenekian, M.; Even, J.; De Siena, M. C.; Klepov, V. V.; Friedrich, D.; Spanopoulos, I.; Tu, Q.; Tajuddin, I. S.; Weiss, E. A.; Kanatzidis, M. G., Thick-Layer Lead Iodide Perovskites with Bifunctional Organic Spacers Allylammonium and Iodopropylammonium Exhibiting Trap-State Emission. *Journal of the American Chemical Society* **2022,** *144* (14), 6390-6409.

47. Huang, B.; Liu, J.; Han, Z.; Gu, Y.; Yu, D.; Xu, X.; Zou, Y., High-Performance Perovskite Dual-Band Photodetectors for Potential Applications in Visible Light Communication. *ACS Appl Mater Interfaces* **2020,** *12* (43), 48765-48772.

48. Bao, C.; Zhu, W.; Yang, J.; Li, F.; Gu, S.; Wang, Y.; Yu, T.; Zhu, J.; Zhou, Y.; Zou, Z., Highly Flexible Self-Powered Organolead Trihalide Perovskite Photodetectors with Gold Nanowire Networks as Transparent Electrodes. *ACS Appl Mater Interfaces* **2016,** *8* (36), 23868-75.

49. Yu, D.; Cao, F.; Gu, Y.; Han, Z.; Liu, J.; Huang, B.; Xu, X.; Zeng, H., Broadband and sensitive two-dimensional halide perovskite photodetector for full-spectrum underwater optical communication. *Nano Research* **2020,** *14* (4), 1210-1217.

50. Deng, H.; Yang, X.; Dong, D.; Li, B.; Yang, D.; Yuan, S.; Qiao, K.; Cheng, Y. B.; Tang, J.; Song, H., Flexible and Semitransparent Organolead Triiodide Perovskite Network Photodetector Arrays with High Stability. *Nano Lett* **2015,** *15* (12), 7963-9.

51. Du, B.; Yang, W.; Jiang, Q.; Shan, H.; Luo, D.; Li, B.; Tang, W.; Lin, F.; Shen, B.; Gong, Q.; Zhu, X.; Zhu, R.; Fang, Z., Plasmonic-Functionalized Broadband Perovskite Photodetector. *Advanced Optical Materials* **2018,** *6* (8), 1701271.

52. Tong, S.; Sun, J.; Wang, C.; Huang, Y.; Zhang, C.; Shen, J.; Xie, H.; Niu, D.; Xiao, S.; Yuan, Y.; He, J.; Yang, J.; Gao, Y., High-Performance Broadband Perovskite Photodetectors Based on $CH_3NH_3PbI_3$/C8BTBT Heterojunction. *Advanced Electronic Materials* **2017,** *3* (7), 1700058.

53. Zhang, Z.; Xu, C.; Zhu, C.; Tong, X.; Fu, C.; Wang, J.; Cheng, Y.; Luo, L., Fabrication of $MAPbI_3$ perovskite/Si heterojunction photodetector arrays for image

sensing application. *Sensors and Actuators A: Physical* **2021,** *332*, 113176.

54. Li, C.; Li, J. X.; Li, C. Y.; Wang, J.; Tong, X. W.; Zhang, Z. X.; Yin, Z. P.; Wu, D.; Luo, L. B., Sensitive Photodetector Arrays Based on Patterned $CH_3NH_3PbBr_3$ Single Crystal Microplate for Image Sensing Application. *Advanced Optical Materials* **2021,** *9* (15), 2100371.

55. Lan, C.; Dong, R.; Zhou, Z.; Shu, L.; Li, D.; Yip, S.; Ho, J. C., Large-Scale Synthesis of Freestanding Layer-Structured PbI_2 and $MAPbI_3$ Nanosheets for High-Performance Photodetection. *Adv Mater* **2017,** *29* (39), 1702759.

56. Du, B.; Lin, L.; Liu, W.; Zu, S.; Yu, Y.; Li, Z.; Kang, Y.; Peng, H.; Zhu, X.; Fang, Z., Plasmonic hot electron tunneling photodetection in vertical Au-graphene hybrid nanostructures. *Laser & Photonics Reviews* **2017,** *11* (1), 1600148.

57. Cao, F.; Yan, T.; Li, Z.; Wu, L.; Fang, X., Dual-Band Perovskite Bulk Heterojunction Self-Powered Photodetector for Encrypted Communication and Imaging. *Advanced Optical Materials* **2022**, *10*(18), 2200786.

58. Feng, F.; Wang, T.; Qiao, J.; Min, C.; Yuan, X.; Somekh, M., Plasmonic and Graphene-Functionalized High-Performance Broadband Quasi-Two-Dimensional Perovskite Hybrid Photodetectors. *ACS Applied Materials & Interfaces* **2021**, (51), 61496-61505.